Investigating the Real Structure of Intermetallic Phases and Nanomaterials by High-Resolution Transmission Electron Microscopy

Reiner Ramlau[#], Wilder Carrillo-Cabrera, Uta Köhler, Sebastian Schwinger, Paul Simon, Iryna Zelenina, Yuri Grin

The Dresden Grand Atomic Resolution Microscope (ARM) was installed at the Department of Chemical Metals Science in 2014. Since then, transmission electron microscopy with atomic resolution has been successfully integrated into the department's multifaceted materials-based research projects, chiefly concerning intermetallic phases as well as oxides, carbides and carbonaceous nanomaterials. Atomic resolution microscopy is complemented by "conventional" high-resolution electron microscopy, electron diffraction, energy-dispersive X-ray spectroscopy and electron energy-loss spectroscopy. Selected methodical studies were performed with partner companies and universities.

The Dresden Grand ARM

During the period under review, the TEM resolution of our JEM-ARM300F (Fig. 1) – nick-named the "Grand ARM" – was even further improved by the manufacturer JEOL. Mechanical re-adjustment of the TEM (image) corrector resulted in decreasing residual fourth-order axial coma aberration (P5). Eventually, both correctors, TEM (image) and STEM (beam), as well as the Gatan imaging filter (GIF) were arranged for an acceleration voltage of 200 kV. Having available the set-up for a third voltage (80 kV, 200 kV and 300 kV) enables us to investigate more materials under their particular optimum conditions.

Fig.-1: The Dresden Grand ARM, the JEM-ARM300F with double C_S-correction by JEOL – nick-named the "Grand ARM" – in its custom-built booth.

Disorder in Clathrates

A comprehensive study by inelastic neutron scattering [1] was devoted to the direct quantitative measurement of phonon lifetimes in a single crystal of the clathrate-I $Ba_{7.81}Ge_{40.67}Au_{5.33}$. The material is known for its puzzling "glass-like" thermal conductivity. The study showed, however, that thermal transport is dominated by acoustic phonons with long lifetimes. This unusual behaviour is caused by the crystal structure allowing only a small number of phonons to form. Extensive crystal growth experiments were performed to get the single crystal suitable for the diverse measurements (see report Baitinger). Eventually, this very single crystal was used to investigate structural disorder with atomic resolution. Aberration-corrected STEM (AC-STEM) reveals that Ba2 and Au/Ge1 atoms are indeed displaced from their ideal positions, resulting in deviations from the translational symmetry with a wide spectrum of characteristic distances (Fig. 2).

$K_7B_7Si_{39}$ was the first borosilicide to be synthesized. Together with the related quaternary borosilicides $K_xMe_yB_7Si_{39}$ (Me: Rb,Cs,Na; $x + y \leq 7$) they are the only clathrates known with boron as host atoms. The presence of boron in the host framework may lead to a considerable deformation of the clathrate cages. It may influence the occupancy of the small (dodecahedra) and large (tetrakaidecahedra) cages with guest atoms and cause displacements of the guest sites from the cage centers. Since, e.g., the $K_7B_7Si_{39}$ compound exhibits lateral Si—Si and Si—K down to 47 pm and 43 pm when projected along prominent zone axes [100] and [111], respectively (Fig. 3a), the borosilicides are striking examples for the need of AC-TEM and -STEM [2].

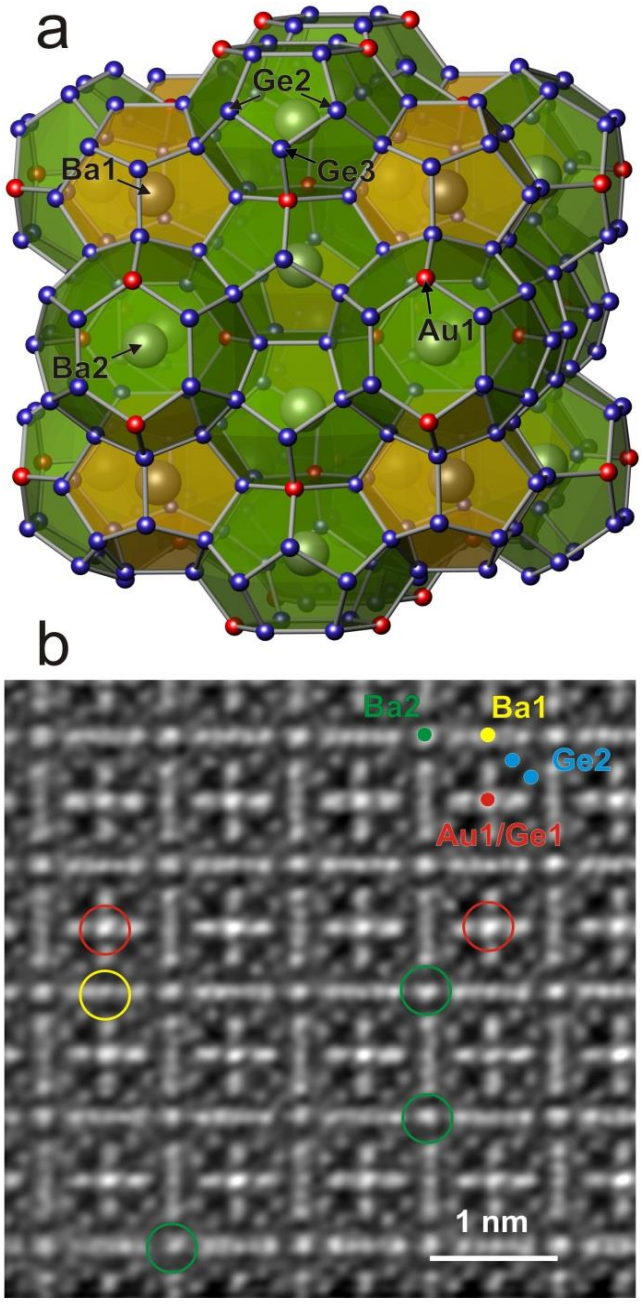

Fig.-2: Crystal structure and local atomic arrangements of $Ba_{7.81}Ge_{40.67}Au_{5.33}$. (a) Ordered clathrate-I model with the composition $Ba_8Ge_{40}Au_6$ showing the Ge/Au framework with dodecahedra (orange) and tetrakaidecahedra (green), occupied by Ba1 (Wyckoff site 2a, yellow) and Ba2 (6d, green) atoms, respectively. Au1 atoms at the 6c site are shown in red. (b) AC-STEM (HAADF) image along the [100] zone axis illustrates the strong displacement of atoms from their ideal positions in the regions of Ba2 (green) and Au1/Ge1 (red) positions in comparison with the Ba1 ones (yellow).

With respect to the ordering of B atoms at the 16i site (green in Fig. 3a), with 2 atoms per unit cell (1 nm) in the columns, the expected contrast differences are very small; they would be enhanced in case of any ordering.

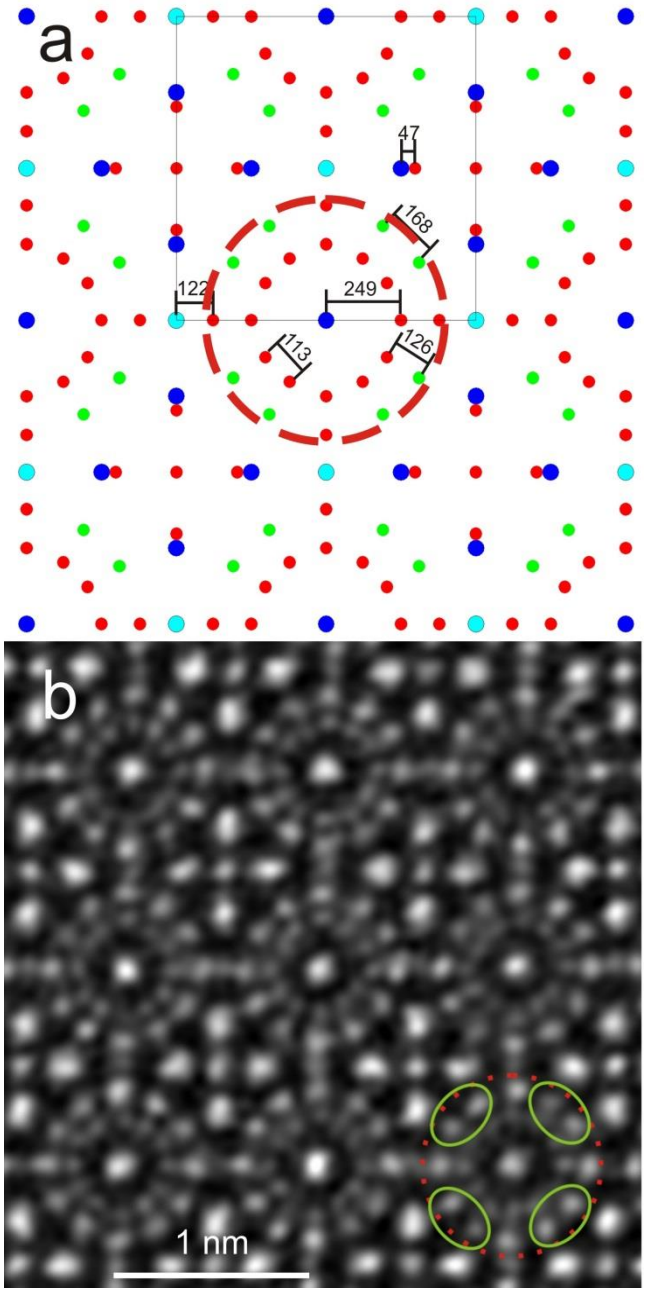

Fig.-3: (a) Projected structure of $K_7B_7Si_{39}$ in [100] direction. The unit cell and some Si—Si, Si—B/Si, and Si—K interspaces (pm) are indicated. Green: (B/Si) at 16i, red: Si at 24k and 6c, light-blue: K at 2a (centre of the small, dodecahedral cage) and dark-blue: K at 6d (centre of the large, tetrakaidecahedral cage). (b) HAADF-STEM image. Along the outer ring of the rose-like features (marked red dotted) Si at 24k and B/Si at 16i are alternating. (Compare the projected structure!) Distinct contrast variations can be noticed between adjacent 16i sites (encircled green) as well as between some of the 16i sites and the 24k sites (always occupied by Si).

On the other hand, by HAADF-STEM (Fig. 3b) the presence of boron, i.e. the lack of silicon, at the respective sites could be imaged directly.

Local Atomic Arrangements in Boron Carbide

One of the seemingly best-known binary ceramic materials was still lacking a coherent description of its crystal structure and physical properties. By combining meticulous *ab initio* computational studies, precise crystal structure determination from diffraction experiments and AC-TEM, a concerted investigation [3] revealed the interaction of hitherto unknown local structure modifications with the already known ones. The mixture of different local atomic arrangements within the real crystal structure reduces the electron deficiency of the pristine CBC + B_{12} structure and introduces new electronic states within the band gap. The question about the electron-precise character of boron carbide could be answered and better understanding of the physical properties established (see report Leithe-Jasper). With respect to atomic-resolution imaging, the particular challenge consisted in the projection problem and possible beam damage. Even when the thickness of the specimen imaged along [211] direction is considered to be very small, e.g. 3.1 nm, six entities (chains and icosahedra) are projected onto each other, thus leading to a mixed image of ideal and modified atomic arrangements. Plenty of different local atomic arrangements had to be generated, partly in large super-cells, and TEM image simulation was performed. Selected local atomic arrangements are shown in Fig. 4.

Revisiting Hollandites

The AC-TEM/STEM study of the hollandite $Bi_xV_8O_{18}$ – in cooperation with the group of A. Maignan ENSICAEN (Caen, France) – revealed the presence of additional V species located in the channels of the crystal structure, together with the Bi. The V fillers occupying off-centre atomic positions in the channels have tetrahedral coordination, whereas the coordination of V is octahedral in the V_8O_{16} framework. A new chemical formula $Bi_{2-y}V_yV_8O_{16}$ was proposed for this hollandite structure [4].

Characterization of Thin Film Displacements

A very careful methodical study on thin film displacements in the electron microscope was made in international cooperation – including JEOL, the manufacturer of the Dresden Grand ARM. The cleanest specimens are often obtained by dispersing micro-crystallites on a thin carbonaceous film. Experimental measurements of the contrast of single atoms indicate, however, fluctuations in the film along the z direction, which may influence the resolution [5].

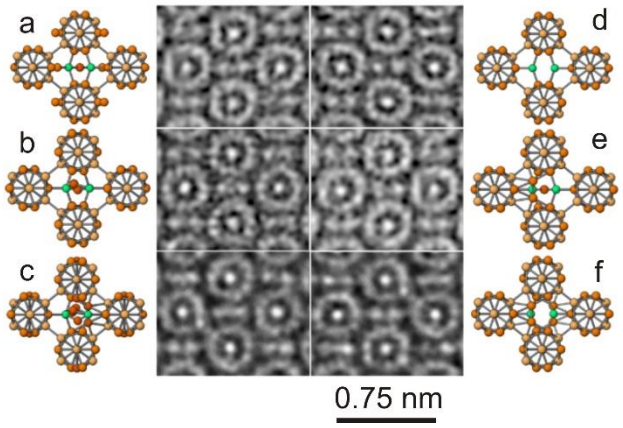

Fig.-4: Local atomic arrangements in the chain region with the main contributions of: a) 4-atomic chains combined with linear chains CBC; b) defect chain C□C; c) bent chains CBC with different orientation of singular chains with respect to projection direction; d) linear chain combined with rhombus CB_2C; e) bent chains CBC combined with the rhombi CB_2C; f) rhombi CB_2C.

Nanopatterned Carbon from Inorganic Precursor Li_2C_2

The precursor Li_2C_2 was synthesized by a solid state reaction of graphite and elemental lithium. After its treatment with SnI_4 the final solid carbon product is amorphous and contains only traces of Li [6]. Redox preparation was also applied to Si analogues [7] and other intermetallic compounds (see report Böhme). The polycrystalline Li_2C_2 shows surface patterning as fine striation of the particles between 200-500 nm. The stratification pattern is characteristic of twinning in the material. TEM investigations revealed a nano-patterning of the amorphous carbon material. At higher magnification, parallel aligned column-like bands were observed with their size in the range of 200-500 nm (Fig. 5a). Inside the bands, tilted nano-stripes of about 50-100 nm were resolved. These stripes in the vicinal bands are oriented opposite to each other and produce a zig-zag or herring-bone pattern, which stems from the twinning of the Li_2C_2 precursor crystal lamellae. Fig. 5b displays the columnar pattern of micro-twinned bands and nano-twinning inside. The sample thickness of 15 nm was determined by tilting experiments. Obviously, the submicron-sized twinning stems from the Li_2C_2 precursor phase and is kept in the carbonaceous oxidation product. Using high-resolution TEM, randomly distributed sub-nanometer sized cavities were observed. At the edge of the sample, loops were visualized indicating initial states for the formation of the pores. The pore diameters mainly range between

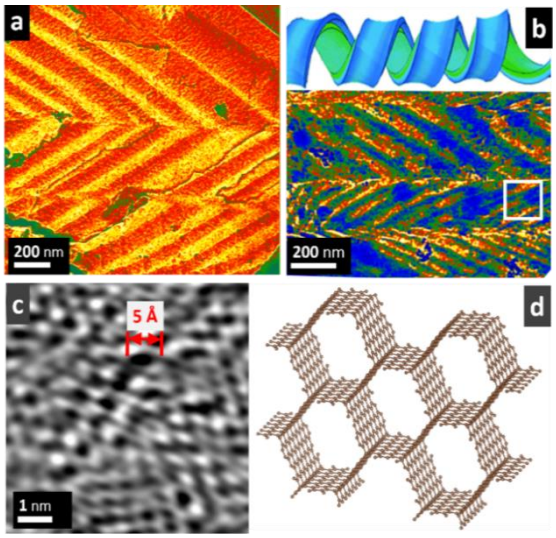

Fig.-5: (a) TEM overview image of an amorphous nano-patterned carbon plate showing large twinning bands of 0.5-1 µm diameter and a tilt angle of 37°. (b) Columnar bands of different sizes. (c) Paracrystal-like ordering of pores. The sample forms a network of pores in the range of 0.2−0.6 nm. (d) Model of graphitic foam with 3×3 phenyl groups as building block.

0.2-0.6 nm. At certain regions, the pores are fused and a paracrystal-like ordered pattern of the pores becomes evident in the Fourier-filtered images (Fig. 5c). Larger pores with ~0.5 nm in diameter dominate giving rise to necklace-like strings besides the presence of smaller pores with sizes between 0.3-0.2 nm. The Fourier transform reveals diffuse "reflections" at 0.94 nm and 0.54 nm in the small-angle region (not shown).

This kind of ordering corresponds to a graphitic foam structure, as suggested by Raman investigations. Carbon foams are hypothetical carbon allotropes that contain graphite-like aromatic sp^2 phenyl group segments, connected by sp^3 carbon atoms, resulting in porous structures. The foam forms a network where the number of phenyl groups between the connecting points determines the size of the meshes. In Fig. 5d a hypothetic 3x3 mesh foam network is shown.

Aluminium in Single Crystals of the Super-conductor UBe_{13}

Already since 1983, the possibility of Al incorporation into the UBe_{13} structure and its effect on its superconductive and other properties has been hotly debated and remained unanswered yet. For example, it was observed that with decreasing lattice parameter a and less Al content the critical temperature T_c is elevated. UBe_{13} crystals show cubic symmetry $Fm\bar{3}c$ with lattice parameter a = 1.025 nm. We investigated

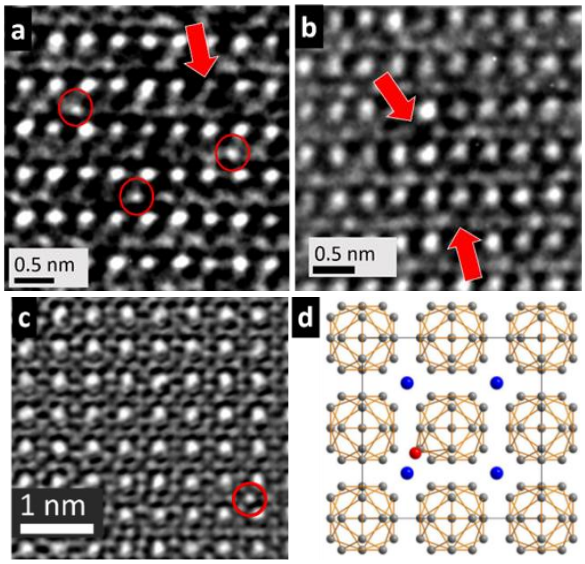

Fig.-6: (a) High-resolution image of as-grown (non-annealed) $UBe_{13-x}Al_x$ single crystal, [110] zone. Aluminium atoms situated on the Be sites are marked by red circles. The strong bright spots indicate uranium. The red arrow points to a uranium vacancy (point defect). (b) Be vacancies indicated by arrows. (c) [100] zone: After 38 days of annealing. Less Al content (red circle, bottom) and lower amount of Be vacancies are detected. (d) Model of UBe_{13} (U blue, Be grey) with Al insertion (red).

as-prepared and annealed samples (38 days @ 900°C). In the as-prepared sample, a high content (~1 at. %) of built-in Al is expected whereas the annealed sample should have lost almost all aluminium. As shown in the high-resolution image of the [110] zone of the as-prepared sample, Al atoms are situated on the Be site, "interstitial" between the uranium layers, marked with red circles. Additionally, vacancies on the Be and U sites were detected, see red arrows (Figs. 6a,b) [8].

Long-term annealing leads to a uniform Al depletion and a healing of the Be vacancies as shown by TEM (Fig. 6c). The model of [100] zone with built-in Al is shown in Fig. 6d. The annealing time needed to reach the highest T_c scales with the crystal dimensions, confirming that Al diffuses and leaves the crystal rather than ordering locally on a specific site (see report Svanidze).

References

[1] *Direct measurement of individual phonon lifetimes in the clathrate compound $Ba_{7.81}Ge_{40.67}Au_{5.33}$. P.-F Lory, S. Pailhès, V. M. Giordano, H. Euchner, H. D. Nguyen, R. Ramlau, H. Borrmann, M. Schmidt, M. Baitinger, M. Ikeda, P. Tomes, M. Mihalkovic, C. Allio, M. R. Johnson, H. Schober, Y. Sidis, F. Bourdarot, L. P. Regnauls, J. Ollivier, S. Paschen, Y. Grin and M. de Boissieu, Nature Communications **8** (2017) 491.*

[2] *Atomic resolution microscopy of intermetallic clathrates, R. Ramlau, Y. Grin and H. Sawada, JEOL News* ***51[1]*** *(2016) 2.*

[3] *Local atomic arrangements and band structure of boron carbide, K. Rasim, R. Ramlau, A. Leithe-Jasper, T. Mori, U. Burkhardt, H. Borrmann, W. Schnelle, C. Carbogno, M. Scheffler and Y. Grin, Angew. Chem. Int. Ed.* ***57*** *(2018) 6130.*

[4] *Revisiting Hollandites: Channels filling by main-group elements together with transition metals in* $Bi_{2-y}V_yV_8O_{16}$*, O. I. Lebedev, S. Hebert, V. Roddatis, C. Martin, S. Turner, A. V. Krasheninnikov, Y. Grin and A. Maignan, Chem. Mater.* ***29*** *(2017) 5558.*

[5] *Characterization of thin film displacements in the electron microscope, H. Sawada, R. Ramlau, C. S. Allen and A. I. Kirkland, Appl. Phys. Lett.* ***111*** *(2017) 203104.*

[6] *Redox route from inorganic precursor* Li_2C_2 *to nano-patterned carbon, P. Simon, X.-J. Feng, M. Bobnar, P. Höhn, U. Schwarz, W. Carrillo-Cabrera, M. Baitinger and Y. Grin, ACS Nano* ***11 [2]*** *(2017) 1455.*

[7] *An amorphous phase of zinc and silicon at composition* Zn_2Si_5*(:H, OH), X. Feng, B. Böhme, M. Bobnar, P. Simon, W. Carrillo-Cabrera, U. Burkhardt, M. Schmidt, U. Schwarz, M. Baitinger, T. Straßner and Y. Grin, Z. Anorg. Allg. Chem.* ***643*** *(2017) 106.*

[8] *Tracking aluminium impurities in single crystals of the heavy-fermion superconductor* UB_{13}*, A. Amon, I. Zelenina, P. Simon, M. Bobnar, M. Naumann, E. Svanidze, F. Arnold, H. Borrmann, U. Burkhardt, W. Schnelle, E. Hassinger, A. Leithe-Jasper and Y. Grin, Sci. Rep.* ***8*** *(2018) 10654.*

[#] Reiner.Ramlau@cpfs.mpg.de